

Electron spin-lattice relaxation of silver nanoparticles embedded in SiO₂ and TiO₂ matrices

G. Mitrikas, C. C. Trapalis, and G. Kordas

Citation: *The Journal of Chemical Physics* **111**, 8098 (1999); doi: 10.1063/1.480143

View online: <http://dx.doi.org/10.1063/1.480143>

View Table of Contents: <http://scitation.aip.org/content/aip/journal/jcp/111/17?ver=pdfcov>

Published by the [AIP Publishing](#)

Articles you may be interested in

[Spin dynamics simulation of electron spin relaxation in Ni²⁺\(aq\)](#)

J. Chem. Phys. **141**, 014109 (2014); 10.1063/1.4885050

[Electron spin-lattice relaxation of low-symmetry Ni²⁺ centers in LiF](#)

Appl. Phys. Lett. **104**, 252902 (2014); 10.1063/1.4885381

[Molecular structure and dynamics of off-center Cu²⁺ ions and strongly coupled Cu²⁺ – Cu²⁺ pairs in BaF₂ crystals: Electron paramagnetic resonance and electron spin relaxation studies](#)

J. Chem. Phys. **127**, 124705 (2007); 10.1063/1.2768518

[Temperature dependence of spin-spin and spin-lattice relaxation times of paramagnetic nitrogen defects in diamond](#)

J. Chem. Phys. **109**, 8471 (1998); 10.1063/1.477511

[Effect of boson peak on low-temperature electron spin–lattice relaxation in amorphous materials](#)

Low Temp. Phys. **24**, 198 (1998); 10.1063/1.593570



Electron spin-lattice relaxation of silver nanoparticles embedded in SiO₂ and TiO₂ matrices

G. Mitrikas, C. C. Trapalis, and G. Kordas^{a)}

Institute of Materials Science, NCSR Demokritos 15310, Aghia Paraskevi, Athens, Greece

(Received 15 January 1999; accepted 6 August 1999)

Metallic silver nanoparticles were prepared by the sol-gel method in amorphous SiO₂ and crystalline TiO₂ matrices. The metal particles were monodispersed in size and their mean diameters varied between 1 and 10 nm, depending upon the processing conditions. The spin-lattice relaxation (SLR) times were investigated by pulsed electron paramagnetic resonance (EPR) spectroscopy in a temperature range between 4 K and 300 K. The spin echo recoveries were slow enough (of the order of some ms), and demonstrated a biexponential character. This study showed that for silver nanoparticles in the SiO₂ matrix, the temperature dependence of T_1 can be described by the relation $(1/T_1) \propto T^n$, where $0.4 < n < 1$. Contrary to this behavior, the temperature dependence of T_1 has a Raman-type character ($1/T_1 \propto T^2$) for silver nanoparticles in the TiO₂ matrix. The unusual behavior for the SiO₂ samples is attributed to the amorphous phase of the SiO₂ matrix. The results are discussed in terms of possible relaxation mechanisms suggested by Khaliullin and Khusainov taking into account the energy levels correlation functions. This study showed that the spin relaxation due to static defects is in agreement with our results. In addition, a satisfactory agreement between theory and experiment can only be obtained in the case of repulsion between the energy levels indicative for the quantum size effect. © 1999 American Institute of Physics. [S0021-9606(99)70741-5]

I. INTRODUCTION

The physical properties of metallic nanoparticles differ from those of bulk samples due to the discrete nature of the electronic energy levels. This fact makes the theoretical and experimental study of these systems a very interesting field of research for the last two decades.¹

The basic properties of small metallic particles are determined by the discrete energy spacing Δ between adjacent levels,

$$\delta = \frac{4E_F}{3N} \propto \frac{1}{V}, \quad (1)$$

where δ is the mean energy spacing between adjacent levels, E_F is the Fermi energy, N is the number of conduction electrons, and V is the volume of the particle. When this energy spacing becomes greater than kT or the Zeeman splitting $\hbar\omega_z$, quantum sized effects are expected to be manifested.²

One of the open questions in the physics of metallic nanoparticles is how the quantization of the energy spectrum influences the relaxation of electron spins. When the size of the particles become very small,³ it is expected that the Elliott mechanism⁴ which is responsible for spin-lattice relaxation (SLR) of conduction electrons in metals should be quenched. Therefore, the study of small metallic particles in terms of SLR of conduction electrons can reveal relaxation processes that are masked in the bulk metal by the electron-phonon scattering.

Furthermore, one of the main unresolved points is whether the energy levels are randomly distributed or they follow a specific distribution function (orthogonal, symplectic or unitary).^{5,6} In the case of paramagnetic nanoparticles, the temperature dependence of the electron SLR is sensitive to the energy levels that exist near the ground state and this can be used as a probe for the study of the energy levels distribution. In addition, the putative dependence of the energy levels on the size of the particles is not clearly understood.

Continuous wave electron paramagnetic resonance (cw-EPR) has been used in the past for the investigation of quantum size effects in metallic nanoparticles.¹ Recently,⁷ we were able to observe cw-EPR from silver nanoparticles embedded in the SiO₂ matrix. However, in this case the interpretation of the results is qualitative because the inhomogeneous effects are always large for small metallic particles.⁸

Pulsed EPR is the most direct technique for the determination of the electron spin lattice relaxation of metallic nanoparticles. In some cases,^{9,10} the suppression of spin relaxation in these systems has been observed using the spin echo method, but to the best of our knowledge, there is no systematic study on the temperature dependence of the SLR times (T_1). Here, we present a detailed study of the SLR times (T_1) of Ag nanoparticles at temperatures between 4.2–300 K. The nanoparticles were embedded in SiO₂ and TiO₂ matrices prepared by the sol-gel method. The observed temperature dependence is discussed in terms of possible relaxation mechanisms.

^{a)} Author to whom correspondence should be addressed. Electronic mail: gkordas@ims.demokritos.gr

II. EXPERIMENT

A. Sample preparation

The Ag particles were prepared by the sol-gel method, which allows the preparation of samples with narrow particle size distributions and adjustable metal loadings.^{11,12} The procedure includes three steps. The first step includes complexation of y equivalents of the silicon alcoxide $\text{NH}_2-(\text{CH}_2)_3-\text{Si}-(\text{OEt})_3$ with 1 equivalent of AgNO_3 and addition of x equivalents of $\text{Si}(\text{OEt})_4$ (TEOS). The hydrolysis and polycondensation of the $\text{Si}-(\text{OEt})$ groups occurs in addition of aqueous suspension of ammonia. During the sol-gel processing, the organic groups $-\text{NH}_2$ coordinate to the metal ions and the resulting metal complexes are anchored to the silicate matrix. In this way, aggregation of the metal ions is prevented and a relatively homogeneous distribution throughout the SiO_2 matrix is succeeded. In the second step, the metal-complex containing gel is dried and then heated in air to oxidize all organic moieties. Thus, small silver oxide particles are formed. In the final step, the composites $\text{Ag} \cdot (x+y)\text{SiO}_2$ are prepared by reduction of the metal oxide particles under hydrogen.

Oxidation and reduction temperatures were determined by differential thermal analysis (DTA) measurements carried out in the first step of preparation. The optimization of the heat treatment conditions was also studied by x-ray diffraction measurements (XRD D500 Siemens). The size of the particles was determined by transmission electron microscopy (TEM CM 20 Phillips). A number of 3 or 4 bright field micrographs were taken for each sample. From these micrographs, a representative number of nanoparticles (500–600) was measured in order to find their size distribution.

B. Spectroscopic measurements

cw-EPR measurements were performed with a Bruker ESP 380 X-band spectrometer. The temperature was varied in the range 4.2–300 K using an Oxford liquid helium flow system. The microwave frequency was measured with a microwave frequency counter HP 5350B.

Pulsed EPR was performed with a Bruker ESP 380 spectrometer. The field swept spectra were obtained by recording the amplitude of the echo as a function of the magnetic field after a two-pulse sequence ($\pi/2$ -320 ns- π); the duration of the $\pi/2$ and π pulses were 64 and 128 ns, respectively.

SLR times, T_1 , were measured by saturation recovery as described in Ref. 13. The saturation recovery was monitored by recording the two-pulse echo intensity ($\pi/2$ -160 ns- π ; with $t_{\pi/2} = 16$ ns) as a function of the time after a saturating pulse sequence. The magnetic field corresponded to the maximum of field swept spectrum. To minimize contributions from spectral diffusion, a burst of N saturating pulses was employed.^{14,15} The pulse length was $t_p = 16$ ns corresponding to $H_1 \approx 6$ G; typically $N = 30$ pulses with an inter-pulse delay of $0.5 \mu\text{s}$ were used. The repetition rate was adjusted in every measurement in order to ensure complete magnetization recovery.

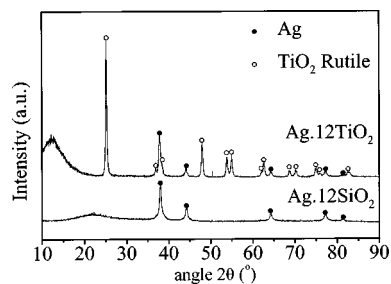


FIG. 1. XRD diagrams of samples S_1 (amorphous) and S_2 (crystalline).

III. RESULTS

The DTA measurements showed a peak at 500°C due to Ag crystallization. This result was confirmed by XRD measurements. Figure 1 shows the XRD diagrams for the two samples heated at 500°C . These diagrams show clearly that the crystalline phase of metallic silver exists in both samples. The additional peaks appearing in the diagram of the sample S_2 correspond to the crystalline phase “anatase” of the TiO_2 network. The XRD investigation demonstrated that the matrix of $\text{Ag} \cdot 12\text{SiO}_2$ and $\text{Ag} \cdot 12\text{TiO}_2$ samples are amorphous and crystalline, respectively.

Figure 2 shows the particle size distributions derived from the analysis of TEM micrographs. The histograms in these figures were obtained from the measurements of $N = 600$ particles. The mean diameter of particles in the samples S_1 and S_2 is 3.2 nm and 3.8 nm, respectively. The size distributions are fairly narrow for both samples. The solid lines in Fig. 2 correspond to the fitting curves calculated by the log-normal distribution function (LNDF),¹⁶

$$\Delta N = \frac{N}{\sqrt{2\pi} \ln \sigma} \frac{1}{d} \exp \left[-\frac{1}{2} \left(\frac{\ln(d/d_0)}{\ln \sigma} \right)^2 \right] \Delta d, \quad (2)$$

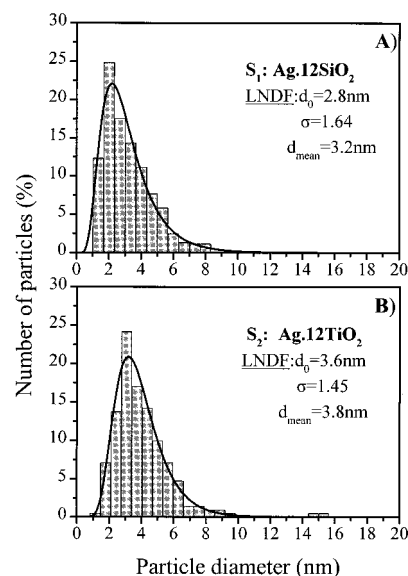


FIG. 2. Size distribution histograms with $\Delta d = 0.65$ nm determined counting $N = 600$ particles. The fitting curves were estimated using LNDF as defined in Eq. (2).

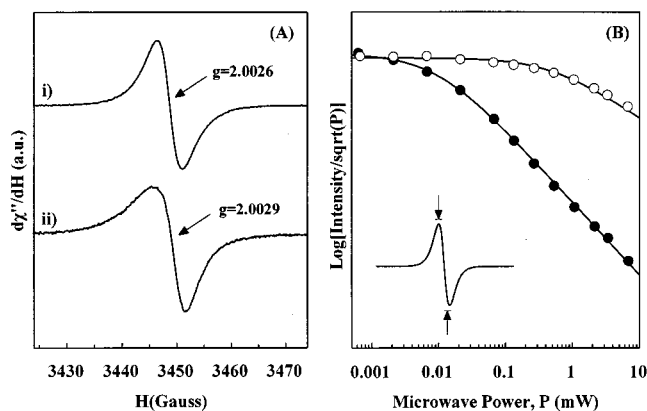


FIG. 3. (A) cw X-band EPR spectra of sample S_1 (i) and sample S_2 (ii). Experimental conditions: temperature, 10 K; microwave frequency, 9.7 GHz; microwave power, 213 nW; modulation frequency, 1.6 kHz; modulation amplitude, 1.5 G. (B) Progressive saturation of the intensity of the first-derivative EPR signal of sample S_1 (open circles) and S_2 (filled circles). The continuous lines are fits using the equation $I = K/(1 + P/P_{1/2})^{b/2}$, where P is the microwave power; for parameters compare text.

where $\Delta N/N$ is the fraction of particles in the interval $\ln(d/d_0)$, $\ln(d/d_0) + \Delta \ln(d/d_0)$; d_0 is the peak diameter of the distribution, σ is a parameter that determines the width of the distribution, and N is the total number of the measured particles in the sample.

Figure 3(A) shows the cw EPR signals recorded for the two samples S_1 (I) and S_2 (II). Each spectrum consists of a structureless derivative with $\Delta H_{pp} = 4.6 \pm 0.5$ G (S_1 , sample) and $\Delta H_{pp} = 6.1 \pm 0.5$ G (S_2 , sample). In a previous study, it was demonstrated that the signal is due to a spin state $S = 1/2$.⁷ The double integral of the signal follows a Curie temperature dependence.⁷ Hyperfine splitting was not observed due to a possible interaction between the spin state with the nucleus of silver ($I = 1/2$).

Progressive microwave saturation can be used to determine relative spin relaxation rates. The saturation curve is constructed by plotting the ratio of the signal amplitude to the square root of power vs the incident microwave power.¹⁷ The saturation data are fit to the expression $I(P) = (1 + P/P_{1/2})^{-b/2}$, where I is the normalized EPR amplitude divided by the square root of the incident microwave power, and P is the incident microwave power. The $P_{1/2}$, the power at which the signal attains half of its unsaturated value and b the inhomogeneity parameter, are the two fitting parameters. The progressive saturation study of the signal shows that the signal saturates easily with no changes in the line shape. The fit of the data displayed in Fig. 3(B), yields $P_{1/2} = 20 \mu\text{W}$ and $b = 1.9$ for the sample S_1 at $T = 10$ K, and $P_{1/2} = 510 \mu\text{W}$ and $b = 1$ for the sample S_2 at room temperature.

Figure 4(A) shows the echo-detected EPR spectrum of the sample S_1 . The SLR was measured by monitoring the saturation recovery of the two-pulse echo at the field position corresponding to the maximum absorption. Figure 4(B) shows a typical echo-detected saturation recovery curve of Ag nanoparticles in amorphous SiO_2 matrix (sample S_1) at 5 K. The recovery is well described by a double exponential; the residual from the fit is shown at the bottom of the transient. The fit at 5 K gives $T_1 = 2.3$ ms for the one and T_1

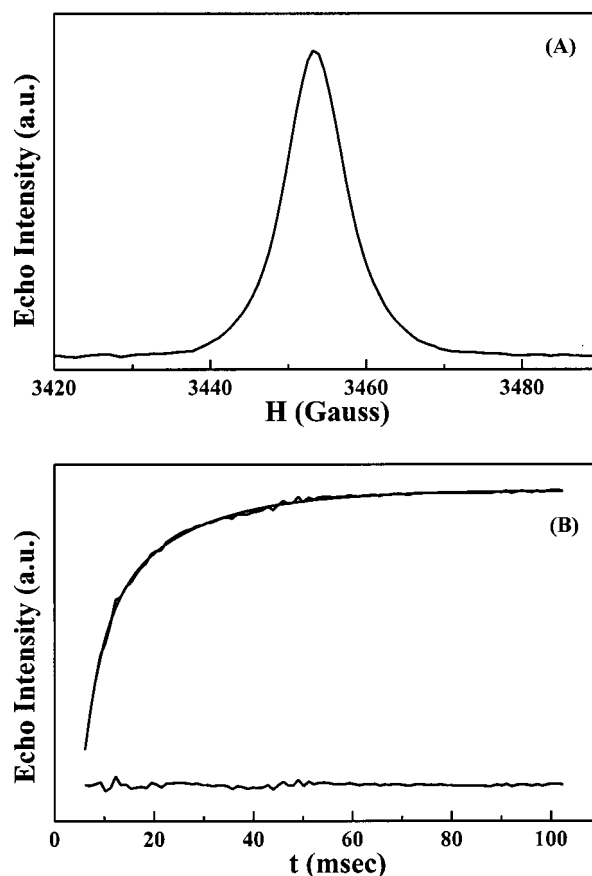


FIG. 4. (A) Amplitude of the electron spin echo of sample S_1 , resulting from a two-pulse sequence, as a function of the magnetic field. Experimental conditions: temperature, 15 K; time interval between successive pulse sets, 50 ms; microwave frequency, 9.7 GHz. (B) Saturation-recovery transient of sample S_1 with the double exponential fit superimposed; the difference between the experimental and the fitted curve is shown at the bottom. Experimental conditions: temperature, 5 K; magnetic field strength, 3453 G; two-pulse repetition time, 240 ms.

$= 12.2$ ms for the other component of the double exponential.

Figure 5 shows the echo-detected saturation recovery curves of Ag nanoparticles in the crystalline TiO_2 matrix (sample S_2) at three different temperatures. The recovery has a biexponential character and at low temperatures is much slower than in the case of sample S_1 . The fit at 12 K gives $T_1 = 36$ ms for the one and $T_1 = 271$ ms for the other component of the double exponential.

We have carefully verified that the fast component is not an artifact caused by spectral diffusion. This test showed that the echo-detected recovery is almost independent on changing the parameters (interpulse delay, pulse duration) of the saturation pulses. In addition, the temperature dependence of the fast component is in disagreement with a temperature independent rate expected for a contribution due to spectral diffusion. This result implies that contributions from spectral diffusion effects are negligible in our samples.

The relaxation measurements were extended over the 5–300 K range for both the amorphous and crystalline samples. The observed SLR rates were double exponential over this range. The two rates have quite the same temperature dependence. The total SLR rate is calculated taking into

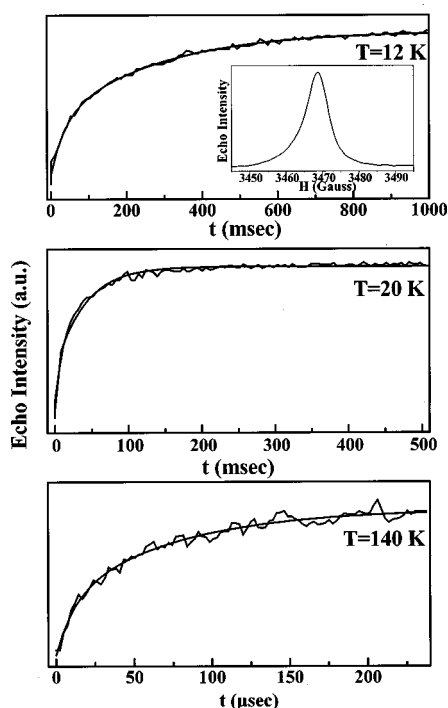


FIG. 5. Saturation recovery transients of sample S_2 at three different temperatures 12 K, 20 K, and 140 K; the double exponential fits are superimposed. Experimental conditions: magnetic field strength, 3469 G; two-pulse repetition time, 960 ms. (Inset) Amplitude of the electron spin echo of sample S_2 , resulting from a two-pulse sequence, as a function of the magnetic field. Experimental conditions: temperature, 10 K; time interval between successive pulse sets, 500 ms; microwave frequency, 9.7 GHz.

account the weight of each component to the total recovery. Figure 6 (filled square) shows the SLR determined as a function of temperature of measurements. The power-law fit of relaxation rates gives a slow temperature dependence of the form $1/T_1 = 0.1 T^{0.6}$. Figure 6 (open square) displays also the temperature dependence of the SLR for the S_2 sample (crystalline). One can perceive from this figure that the temperature dependence of the SLR is stronger in the S_2 sample than

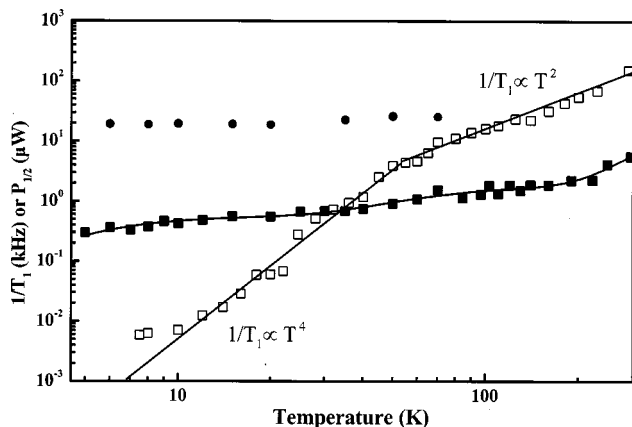


FIG. 6. Filled symbols: temperature dependence of the spin-lattice relaxation rate (filled squares) and determined values of $P_{1/2}$ (filled circles) for the sample S_1 . The solid line is the fit using Eq. (4); for fitting parameters see text. Open squares: temperature dependence of the spin-lattice relaxation rate for the sample S_2 .

in the S_1 sample. For the comparison, the figure shows also the temperature dependence of $P_{1/2}$ for the S_1 sample (filled circles). The power-law fit of relaxation rates gives a Raman-type temperature dependence, which approximates the form $1/T_1 = 0.015T^2$ at temperatures above 60 K.

IV. DISCUSSION

The progressive saturation measurements showed that the inhomogeneity parameter, b , is equal to 1.9 for sample S_1 . For a spin system described by the Bloch equations,¹⁷ the parameter b can be equal to 1 and 3 indicating a completely inhomogeneous and homogeneous broadening character, respectively. The intermediate value of $b = 1.9$ implies that the cw-EPR spectrum of the silver nanoparticles has a modest homogeneous broadening character.¹⁷

It is known that $P_{1/2}$ is inversely proportional to the product $T_1 T_2$.¹⁷ The similar temperature dependence of the $P_{1/2}$ and the T_1 for sample S_1 (Fig. 6 filled squares and circles) indicates that the T_2 for these silver nanoparticles is temperature independent. This implies that the exchange or spin hopping mechanisms cannot account for the SLR temperature variation. Since the temperature variation of the SLR for the amorphous and crystalline samples are different, the interpretation of the experimental finding will be discussed separately.

A. SLR of sample S_1

The measured SLR times of nanoparticles in the sample S_1 are about two orders of magnitude greater than the ones of the bulk metal.¹⁸ This result suggests the freezing of the relaxation process due to the discreteness of the electronic energy spectrum as suggested by Kawabata and Holand.^{3,19} Our data imply that the temperature dependence of the SLR rate is described by an equation of the form $1/T_1 \propto T^{0.6 \pm 0.1}$.

This behavior is rather unusual because it does not agree with any of the well-known SLR processes such as “direct,” “Raman,” and “Orbach–Aminov” processes.^{20–22} In the “direct” process, the relaxation rate $1/T_1$ is proportional to the absolute temperature. For EPR experiments performed at frequencies near 9 GHz, the Zeeman splitting, $\hbar\omega_z$, is about 1 K in temperature units. Thus, at higher temperatures the direct process is rather improbable due to the limited number of phonons with energies close to $\hbar\omega_z$.²¹ As the temperature is raised, other relaxation processes become important. One of them is the inelastic scattering of phonons by the spin, which is generally referred to as the “Raman” process. In this process, the relaxation rates vary as T^6 , T^7 , or T^9 . At high temperatures, all two-phonon relaxation processes vary as T^2 .²⁰ If the system has electronic energy levels lying within the phonon spectrum, it is possible for a spin to relax making transitions between the ground state and the excited states.²² This is a second order process, known as the “Orbach–Aminov” process. The relaxation rate in this case varies as $\Delta^3 / [\exp(\Delta/kT) - 1]$, where Δ is the energy difference between the excited state and the ground states. Among the possible SLR processes, the Orbach–Aminov is the only one that could give direct information about the electronic spectrum of metallic nanoparticles since it is directly related with the energy Δ . When the motion of the matrix atoms

becomes very inharmonic, the Debye model and the concept of lattice phonons are no longer useful in the calculation of the temperature dependence of the SLR rate. In this limit, it is more useful to consider the nuclear motion as described by a correlation function with a correlation time τ_c that is temperature dependent. The SLR may be driven by this motion which produces a modulation of the magnetic interaction between the spin and the nuclei of the glassy solid. Then, the SLR rate has temperature dependence determined by the temperature dependence of τ_c .

The unusual behavior of SLR in sample S_1 may be attributed to the amorphous phase of SiO_2 . Analogous irregularities in the temperature dependence of the SLR time have also been observed for other paramagnetic centers in glassy matrices.^{23–25} In all these cases, the unusual behavior is attributed to the existence of localized-tunneling states,²⁵ which have successfully explained the low-temperature properties of amorphous materials.²⁶ This model assumes that, in a glass, there are a number of atoms or molecules for which the local potential has more than one minimum and thus can be described by an asymmetric double well potential. The tunneling occurs through the barrier separating the two wells. The correlation time for these tunneling modes is given by

$$\tau_c^{-1} \propto E \operatorname{csch}(E/kT), \quad (3)$$

where E is the energy difference between the two positions in the lattice that the nuclei may occupy. This model was used by Kurtz and Stapleton,²⁷ in their effort to explain the unusual temperature dependence of the SLR times of F^+ centers in β -alumina. The temperature dependence is that predicted by Murphy,²⁸ who considered localized vibrational modes instead of tunneling. At temperatures $kT \ll E$, the correlation time varies as $E \exp(-E/kT)$, whereas at high temperatures $kT \gg E$, approximates a linear function of the form $\tau_c^{-1} \propto T$.

Recently, Aminov *et al.*,²⁹ proposed a semiphenomenological generalization of the former model in order to describe the temperature dependence of the SLR times of E'_1 centers in quartz glass. According to this, the relaxation rate is given by

$$T_1^{-1} \propto \frac{\gamma}{\omega_0^2 + \gamma^2} \operatorname{sech}^2 \frac{\Delta}{2T}, \quad (4)$$

where ω_0 is the microwave frequency, and γ is the temperature independent correlation frequency of the random (other than phonon) process causing the relaxation via the two states separated by the energy Δ . We can fit our data using three parameters Δ_1 , Δ_2 , and Δ_3 in Eq. (4). The fitting procedure gives $\Delta_1 = 5$ K, $\Delta_2 = 61$ K, and $\Delta_3 = 604$ K. At present, we cannot correlate these values with some physical parameters of our system since they are associated with the vibrations of the silica atoms and not with the energy levels of the particles. Though, the phenomenological model can qualitatively describe the slow temperature dependence of the observed SLR rates between the range 4–100 K (Fig. 6).

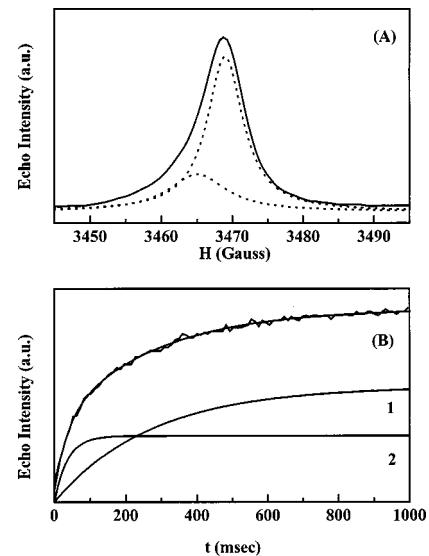


FIG. 7. (A) Simulation of the field swept spectrum of sample S_2 (solid line) with two Lorentzian curves (dotted lines). Experimental conditions: temperature, 12 K; time interval between successive pulse sets, 500 ms; microwave frequency, 9.7 GHz. (B) Saturation recovery transient of sample S_2 with the double exponential fit superimposed ($M(t) = 0.06 + 0.34[1 - \exp(-t/36)] + 0.59[1 - \exp(-t/270)]$). The solid curves are the slow (1) and fast (2) component of the double exponential. Experimental conditions: temperature, 12 K; magnetic field strength, 3469 G; two-pulse repetition time, 960 ms.

B. SLR of sample S_2

For silver nanoparticles embedded in the crystalline matrix of TiO_2 , the SLR dependence is different than the one observed for Ag in the amorphous matrix. In particular, the SLR rates at temperatures below 30 K are several times slower than the corresponding ones in the glass matrix. Above 50 K, these rates have stronger temperature dependence obeying an unusual relaxation process. The difference between the SLR times obtained in S_1 and S_2 samples reinforces the assumption that the unusual temperature dependence of the SLR times in SiO_2 is due to the amorphous phase of the glass matrix.

Important information includes the echo recovery experiments. The progressive microwave saturation measurements showed that the cw-EPR signal is inhomogeneously broadened. This is also evident from the asymmetry of the echo detected EPR signal displayed in Fig. 5 (inset). The spectrum can be fitted with two Lorentzian curves as shown in Fig. 7. One can assume that the biexponential character of the total magnetization recovery is a consequence of two components contributing to SLR times. In this case, the contribution of each exponential component to the total recovery should have the same weight of the corresponding Lorentzian curve in the cw-EPR spectrum. We have performed two-pulse field swept experiments varying the repetition rate of the pulses in order to prove this point. This study showed that the high field components have faster relaxation rates than the corresponding ones in the low field region. Taking into account the weighting factors followed by the EPR signal simulation displayed in Fig. 7(A), it should be expected that the fast relaxation rate would be the dominant factor in

the total magnetization recovery. This hypothesis contradicts the fitting results based on SLR measurements at $T=12$ K, as displayed in Fig. 7(B). Moreover, the same analysis at different temperatures gave analogous results. We concluded that the biexponential character of the magnetization recovery could not be assigned to inhomogeneous broadening effects.

Khaliullin and Khusainov reported a theoretical model accounting for the SLR of conduction electrons in small metallic particles.³⁰ These authors noticed that the electron spin relaxation is the result of coupling of the metal atoms to the insulating medium (matrix). The nature of relaxation depends on the strength of this coupling. In this model the SLR and its temperature dependence are governed by spin-orbit scattering of electrons by thermal vibrations and by inhomogeneities at the metal-matrix interfaces. According to this model, at low temperatures $T < \Delta$, where Δ is the energy spacing between adjacent levels, the recovery is nonexponential and is governed by the nature of the level statistics. The time dependence of the magnetization recovery of the ensemble of the particles is given by the expression

$$M_z(t) = 1 - \int_0^\infty \exp[-t/\tau_{sp}(\omega)] P(\omega) d\omega, \quad (5)$$

with

$$\tau_{sp}^{-1}(\omega) = A \frac{(\omega/2T)^\alpha}{\text{sh}(\omega/2T)[4 + \text{sh}^2(\omega/2T)]^{1/2}}, \quad (6)$$

where ω is the energy difference between the neighboring levels, and $P(\omega)$ is the correlation function that governs the energy spectrum.² The values of the relaxation parameter A and of the exponent α , depend on the strength of metal-insulator interaction. At high temperatures $T > \Delta$, this model predicts that in the case of strong coupling the relaxation is irrespective of the nature of the statistic of the levels and the total magnetization decays exponentially with a relaxation time equal to its value for a bulk metal. On the contrary, when the coupling is weak, the relaxation process is strongly suppressed also at high temperatures.

Another possible relaxation mechanism is the surface spin relaxation, as considered by this theory.³⁰ The relaxation is driven by the electron-phonon interaction between the spin and static defects that may exist at the surface of the small particle. At low temperatures $T < \Delta$, the temperature dependence of the relaxation parameter A is the same as the previous mechanism, but there is a qualitative difference; in the SLR case $A \propto 1/d^2$, whereas in the surface relaxation case $A \propto d^2$. At high temperatures $T > \Delta$, the temperature dependence of the spin relaxation due to static defects is weaker than that due to lattice vibrations.

The fit of the different models to our data will qualitatively decide which of the case fits our data better and which mechanism may be present in our sample. From the temperature dependence of the parameter A , we can determine whether the phonon spectrum of small particles is continuous (strong coupling) or quasidiscrete (weak coupling). Our results show that at high temperatures the SLR rate varies as T^2 . Moreover, the nonsingle exponential character of the echo recovery is retained even at high temperatures. This

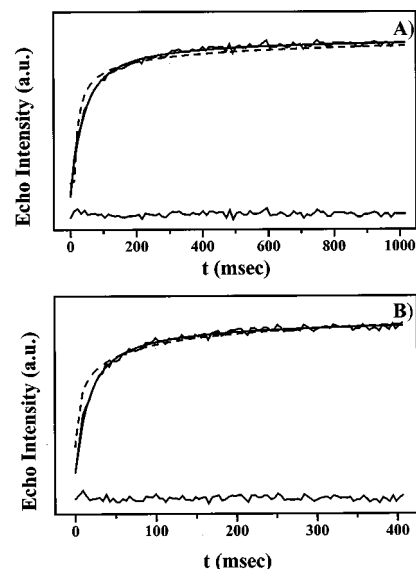


FIG. 8. Saturation recovery transients at $T=15$ K of sample S_2 (A), and another sample with $d_{\text{mean}}=5.4$ nm (B). The solid lines are the fits using Eq. (5) with an orthogonal correlation function defined by Eq. (7); the difference between the experimental and the fitted curves is shown at the bottom; for parameters see text. The dashed lines are the fits using Eq. (5) with a Poisson correlation function $P(\omega) = 1/\delta \exp(-\omega/\delta)$.

behavior implies the suppression of the relaxation process indicative for a weak coupling between the particle and the matrix atoms. Taking into account that a chemical bond between them is rather improbable, the case of a weak coupling is consistent with our results.

It is very important in the context of this model to distinguish between spin-lattice and surface spin relaxation effects. In order to investigate this point, we have performed relaxation measurements at samples with bigger particle diameters. This study showed that these particles have faster relaxation rates as displayed in Fig. 8(B). This result demonstrates that surface spin relaxation effects are dominant in our system.

Following the above qualitative arguments, we can focus our study on the surface spin relaxation case considering a weak coupling between the particles and the matrix. In this special case, at temperatures $T < \Delta$, the relaxation parameter A in Eq. (6) is proportional to T^3 with $\alpha=3$. Inserting these values, we will attempt to fit the experimental recovery curves using Eq. (5) for each one of the three possible correlation functions $P(\omega)$. The fitting results for sample S_2 based on a least-squares fitting procedure are displayed in Fig. 8(A). The fitting parameters are the relaxation parameter A and the mean energy spacing between adjacent levels δ which enters in $P(\omega)$. It is evident from Fig. 8, that a satisfactory agreement can be obtained only in the case of repulsion between the energy levels.⁵ Contrary to this, when a random distribution of levels is applied,² the fitting quality is poor. Moreover, the best fit is obtained if we assume the orthogonal correlation function

$$P(\omega) = \frac{\pi\omega}{2\delta^2} \exp\left(-\frac{\pi\omega^2}{4\delta^2}\right). \quad (7)$$

The fit of our data displayed in Fig. 8(A) gives $\delta = 106$ K. This result can be now compared with the value expected from Eq. (1) taking into account the determined size distribution of the particles. For a LNDF size distribution, we find for the average size distribution $\overline{d^{-3}}$ the value of 0.04. Inserting this value in Eq. (1),¹ we calculate for δ the value of 110 K which is the same within the errors of measurements to the result of the fit to the experimental values [Fig. 8(A)]. The same features are observed in the case of SLR of silver nanoparticles with mean diameter $d = 5.4$ nm. The echo recovery at $T = 15$ K is displayed in Fig. 8(B). The fit gives $\delta = 88$ K. Although this result is in agreement with Eq. (1), we cannot repeat the previous comparison because the size distribution is not monodispersed in this sample.

V. CONCLUSIONS

It follows from the above discussion that the electron SLR study of silver nanoparticles can give information about the interaction with the matrix in which they are located. We show that in the case of silver nanoparticles in SiO_2 , the relaxation process is blocked due to the amorphous phase of the matrix. This study shows that the spin-lattice relaxation of metallic nanoparticles in SiO_2 is not thoroughly understood at present. Moreover, we are not able to use the relaxation model of Khaliullin and Khusainov,³⁰ because it is based on the Debye theory. This picture is completely changed when these particles are embedded in the crystalline matrix of TiO_2 . In this case the temperature dependence of the SLR rates and the nature of the magnetization recovery are in agreement with the predictions of Khaliullin and Khusainov. In the context of this model, we found that the best fitting is achieved when the energy levels repulsion is applied. The results are in good agreement with the experimentally determined parameters.

ACKNOWLEDGMENTS

We thank the Greek General Secretariat for Research and Technology and European Community for funding this research under Contract No. EPIET II 296. We also thank Dr. N. Boukos for the TEM micrographs.

- ¹W. P. Halperin, *Rev. Mod. Phys.* **58**, 533 (1986).
- ²R. Kubo, *J. Phys. Soc. Jpn.* **17**, 975 (1962).
- ³A. Kawabata, *J. Phys. Soc. Jpn.* **29**, 902 (1970).
- ⁴R. J. Elliott, *Phys. Rev.* **96**, 266 (1954).
- ⁵L. P. Gor'kov and G. M. Eliashberg, *Sov. Phys. JETP* **21**, 940 (1965).
- ⁶J. A. A. J. Perenboom, P. Wyder, and F. Meier, *Phys. Rep.* **78**, 173 (1981).
- ⁷G. Mitrikas, C. C. Trapalis, N. Boukos, V. Psycharis, L. Astrakas, and G. Kordas, *J. Non-Cryst. Solids* **224**, 17 (1998).
- ⁸D. A. Gordon, *Phys. Rev. B* **13**, 3738 (1976).
- ⁹Yu. I. Talanov, F. G. Cherkasov, S. F. Chernov, and E. G. Kharakhash'yan, *JETP Lett.* **43**, 435 (1986).
- ¹⁰V. A. Zhikarev, A. P. Staroverov, Yu. I. Talanov, F. G. Cherkasov, and S. F. Chernov, *Sov. Phys. Solid State* **29**, 981 (1987).
- ¹¹B. Breitscheidel, J. Zieder, and U. Schubert, *Chem. Mater.* **3**, 599 (1991).
- ¹²U. Schubert, B. Breitscheidel, H. Buhler, C. C. Egger, and W. Urbaniak, *Mater. Res. Soc. Symp. Proc.* **271**, 621 (1992).
- ¹³Y. Deligiannakis, A. Boussac, and W. A. Rutherford, *Biochemistry* **34**, 16030 (1995).
- ¹⁴R. L. Dalton, L. A. Kwiram, and A. L. Cowen, *Chem. Phys. Lett.* **17**, 495 (1972).
- ¹⁵F. W. Beck, B. J. Innes, and W. G. Brudvig, in *Current Research in Photosynthesis*, edited by M. Baltscheffsky (Kluwer Academic, Dordrecht, The Netherlands, 1990), p. 817.
- ¹⁶C. G. Granqvist and R. A. Burhman, *J. Appl. Phys.* **47**, 2200 (1976).
- ¹⁷C. P. Poole, *Electron Spin Resonance: A Comprehensive Treatise on Experimental Techniques* (Wiley, New York, 1983).
- ¹⁸D. Lubzens, M. R. Shanabarger, and S. Schultz, *Phys. Rev. Lett.* **29**, 1387 (1972).
- ¹⁹B. W. Holland, in *Proceedings of the 14th Colloque Ampere*, Ljubljana, 1996, edited by R. Blinc (North-Holland, Amsterdam, 1967), p. 468.
- ²⁰M. K. Bowman and L. Kevan, in *Time Domain Electron Spin Resonance*, edited by L. Kevan and R. N. Schwartz (Wiley, New York, 1979), Chap. 3, p. 80.
- ²¹A. Abragam and B. Bleaney, *Electron Paramagnetic Resonance of Transition Ions* (Clarendon, Oxford, 1970).
- ²²R. Orbach, *Proc. R. Soc. London, Ser. A* **264**, 458 (1961); L. K. Aminov, *Zh. Eksp. Teor. Fiz.* **42**, 783 (1962).
- ²³D. W. Feldman, J. G. Castle, Jr., and G. R. Wagner, *Phys. Rev.* **145**, 237 (1966).
- ²⁴M. K. Bowman and L. Kevan, *J. Phys. Chem.* **81**, 456 (1977).
- ²⁵G. Kordas, *Phys. Chem. Glasses* **33**, 4 (1992); **33**, 143 (1992).
- ²⁶P. W. Anderson, B. I. Halperin, and C. M. Varma, *Philos. Mag.* **25**, 1 (1972).
- ²⁷S. R. Kurtz and H. J. Stapleton, *Phys. Rev. B* **22**, 2195 (1980).
- ²⁸J. Murphy, *Phys. Rev.* **145**, 241 (1966).
- ²⁹L. K. Aminov, I. N. Kurkin, D. A. Lukoyanov, and K. P. Chernov, *Phys. Solid State* **39**, 1184 (1997).
- ³⁰G. G. Khaliullin and M. G. Khusainov, *Sov. Phys. JETP* **67**, 524 (1988).